CARDIFF UNIVERSITY
PRIFYSGOL CAERDYDD

Online Research @ Cardiff

This is an Open Access document downloaded from ORCA, Cardiff University's institutional repository: https://orca.cardiff.ac.uk/id/eprint/116478/

This is the author's version of a work that was submitted to / accepted for publication.

Citation for final published version:

Ren, Dingkun, Rong, Zixuan, Azizur-Rahman, Khalifa M., Somasundaram, Siddharth, Shahili, Mohammad and Huffaker, Diana L 2018. Feasibility of achieving high detectivity at short- and mid-wavelength infrared using nanowire-plasmonic photodetectors with p-n heterojunctions. Nanotechnology 30 , 044002. 10.1088/1361-6528/aaed5c file

Publishers page: http://dx.doi.org/10.1088/1361-6528/aaed5c
<http://dx.doi.org/10.1088/1361-6528/aaed5c>

Please note:
Changes made as a result of publishing processes such as copy-editing, formatting and page numbers may not be reflected in this version. For the definitive version of this publication, please refer to the published source. You are advised to consult the publisher's version if you wish to cite this paper.

This version is being made available in accordance with publisher policies. See
http://orca.cf.ac.uk/policies.html for usage policies. Copyright and moral rights for publications made available in ORCA are retained by the copyright holders.

information services
gwasanaethau gwybodaeth

Feasibility of Achieving High Detectivity at Short- and Mid-Wavelength Infrared Using Nanowire-Plasmonic Photodetectors with P-N Heterojunctions

Dingkun Ren[1,*], Zixuan Rong[1], Khalifa M. Azizur-Rahman[2], Siddharth Somasundaram[1], Mohammad Shahili[1], and Diana L. Huffaker[1,2,3]

[1] Department of Electrical and Computer Engineering, University of California, Los Angeles, Los Angeles, California, USA, 90095

[2] School of Physics and Astronomy, Cardiff University, Cardiff, Wales, UK, CF24 3AA

[3] California NanoSystems Institute, University of California, Los Angeles, Los Angeles, California, USA, 90095

[*]Email: dingkun.ren@ucla.edu

Abstract

Photodetection at short- and mid-wavelength infrared (SWIR and MWIR) enables various sensing systems used in heat seeking, night vision, and spectroscopy. As a result, uncooled photodetection at these wavelengths is in high demand. However, these SWIR and MWIR photodetectors often suffer from high dark current, causing them to require bulky cooling accessories for operation. In this study, we argue for the feasibility of improving the room-temperature detectivity by significantly suppressing dark current. To realize this, we propose using (1) a nanowire-based platform to reduce the photoabsorber volume, which in turn reduces trap state population and hence G-R current, and (2) *p-n* heterojunctions to prevent minority carrier diffusion from the large bandgap substrate into the nanowire absorber. We prove these concepts by demonstrating a comprehensive 3-D photoresponse model to explore the level of detectivity offered by vertical InAs(Sb) nanowire photodetector arrays with self-assembled plasmonic gratings. The resultant electrical simulations show that the dark current can be reduced by three to four orders at room temperature, leading to a peak detectivity greater than 3.5×10^{10} cm $Hz^{1/2}W^{-1}$ within the wavelength regime of 2.0 – 3.4 μm, making it comparable to the best commercial and research InAs *p-i-n* homojunction photodiodes. In addition, we show that the plasmonic resonance peaks can be easily tuned by simply varying the exposed nanowire height. Finally, we investigate the impact of nanowire material properties, such as carrier mobility and carrier lifetime, on the nanowire photodetector detectivity. This work provides a roadmap for the electrical design of nanowire optoelectronic devices and stimulates further experimental validation for uncooled photodetectors at SWIR and MWIR.

Keywords

Nanowire, plasmonic, photodetector, SWIR, MWIR, detectivity, heterojunction

1. Introduction

III-V semiconductor photodetectors operating at short- and mid-wavelength infrared (SWIR and MWIR at 1.4 – 3 µm and 3 – 5 µm wavelengths, respectively) are the technology of choice for a broad range of imaging applications, such as heat seeking, night vision, remote sensing, and spectroscopy. Achieving uncooled and high-detectivity photodetectors in these wavelength regimes is highly desirable. Uncooled microbolometer focal plane arrays (FPAs) have been commercialized; however, it is more advantageous to develop imagers based on semiconductor-based monolithic and hybrid structures, since they allow for high-speed, compact, and fully integrated sensing platforms. Several examples of commercially available or well-developed uncooled semiconductor detectors (in photovoltaic mode) at SWIR and MWIR include: (1) extended InGaAs *p-i-n* homojunction photodiodes with a peak detectivity between 4.0 – 5.0×10^{10} cm·Hz$^{1/2}$/W and cutoff wavelength of 2.6 µm [1]; (2) InAs *p-i-n* homojunction photodiodes with detection wavelength up to 3.4 µm and detectivity between 4.0 – 5.0×10^{9} cm·Hz$^{1/2}$/W [2,3]; and (3) InAsSb nBn detectors offering a cutoff wavelength at 4.5 µm with detectivity between 1.0 – 2.0×10^{9} cm·Hz$^{1/2}$/W [4]. Clearly, the detectivity decreases with increasing wavelength, resulting from higher dark current from generation-recombination (G-R) process and minority carrier diffusion in small bandgap materials. Although considerable progress has been made in the past decade, there still exists a fundamental limit to achieving higher detectivity due the trade-off between high responsivity and low dark current, as interpreted by a well-known equation (in the quantum regime):

$$D^* = \frac{\sqrt{AB}}{NEP} \approx \frac{R}{\sqrt{2qJ_{dark}}} \tag{1}$$

where D^* is the detectivity, A is the area of detector, B is the bandwidth, NEP is the noise-equivalent power, R is the responsivity, J_{dark} is the dark current density, and q is the elementary charge. Based on eq.1, an obvious solution to increase D^* is by decreasing J_{dark}. However, in practice, this usually involves reducing the absorption layer thickness (reduces trap state population leading a decrease in G-R current), which in turn decreases optical absorption leading to a decrease in R. Thus, the task of overcoming the trade-off

between high responsivity and low dark current to yield higher D^* for SWIR/MWIR photodetectors remains a critical challenge.

To break the trade-off, we must suppress J_{dark} by largely reducing absorption volume, while still maintaining optical absorption within the same order of magnitude. This can be achieved by implementing a plasmonically-enhanced nanowire-based photodetection platform with small fill factor, as shown in figure 1. The nanowire photodetectors are composed of vertically-oriented nanowire arrays with *n*-InAs(Sb) absorber and contact layers grown on large bandgap p^+-InP substrates, along with self-assembled plasmonic gratings (or light couplers). The small fill factor of the nanowire arrays results in a reduced absorber volume, which in turn decreases the contribution of the G-R current and minority carrier diffusion current from the nanowire to the overall device leakage current (J_{dark}). Concurrently, the loss of the optical absorber volume is compensated by using efficient plasmonic light couplers. These couplers strongly couple and confine incident light to surface plasmonic modes in the nanowire top segments and are independent of the nanowire substrate optical property [5,6]. This is advantageous as the overall vertical nanowire height can be as short as possible provided that the exposed nanowire height allows surface plasmonic resonance absorption at the target wavelength. In addition, the InAs(Sb) nanowire-based platform is designed on larger bandgap InP substrates to form *p-n* heterojunctions [7,8], consequently minimizing the contribution of minority carrier diffusion current from the substrate to the saturation current (J_0). If the drop in J_{dark} is more significant than the loss of optical absorption in the nanowire array with a small fill factor, a dramatic enhancement in D^* can be expected. Note that the material system used here cannot be implemented in thin-film growth techniques since the large junction area and lattice mismatch would inevitably cause point and threading dislocations.

To date, several pioneering studies on InAs(Sb) vertical nanowire-based photodetectors at SWIR and MWIR have been reported. These include InAs(Sb) nanowire photodectectors up to ~3.5 μm [9-11] and InAsSb nanowire photodetectors at MWIR [6,12]. More recently, uncooled InAs(Sb) nanowire photodetector arrays with *n*-InAs(Sb)/*p*-InP heterojunctions showed photodetection signatures at both SWIR and MWIR [13,14]. Concurrently, several promising nanowire-based photonic schemes have also

been explored for photodetection at MWIR, including the optimization of HE_{11} waveguide modes for optical absorption in InAs(Sb) nanowires [15-17] and coupled optical modes in InAsSb nanowire clusters [18]. Despite these advances, the true potential of InAs(Sb) nanowire photodetectors as uncooled photodetection platforms has not yet been quantitatively analyzed, and the true limit of their figure-of-merits (R and D^*), remains unclear. In this work, we take a simulation approach to numerically investigate the spectral response of the proposed InAs(Sb) photodetectors with plasmonic metal gratings. Of the various photonic device schemes investigated thus far, nanowire-plasmonic structures offer the unique balance between good electrical contact (ohmic) and enhanced absorption through surface plasmon resonance in the small nanowire volume at SWIR and MWIR. We develop a three-dimensional (3-D) photoresponse model to computationally calculate the photocurrent of the nanowire photodetectors by incorporating simulated optical generation profiles into the electrical models. Then, the simulated dark current and spectral response are compared with the best commercial and research InAs *p-i-n* photodiodes in photovoltaic mode. We show that the dark current can be reduced by three to four orders of magnitude, leading to a peak D^* (on surface plasmonic resonance) greater than 3.5×10^{10} cm $Hz^{1/2}W^{-1}$ within the wavelength regime of 2.0 – 3.4 µm. In addition, we show that the absorption peaks can be freely tuned by varying the exposed nanowire height. Finally, we take the nanowire material quality into account, and analyze the impact of doping level, carrier mobility, and carrier lifetime on peak D^*. Our work provides a solid foundation to inspire further experimental validation efforts in realizing InAs(Sb) nanowire-plasmonic photodetector arrays that accomplish room-temperature photodetection with high D^* at SWIR and MWIR.

2. Modeling and simulation section

2.1. Model setup

A square unit cell with a single InAs(Sb) nanowire at the center was used to a simulate an infinitely extending nanowire array. The nanowire device was then constructed by specifying the passivation shell (Al_2O_3), a dielectric growth mask (SiO_2), a growth substrate (InP), a bisbenzocyclobutene (BCB) layer, a plasmonic grating, and ambient air. BCB is an insulating filler medium that structurally supports the

nanowire top contact and isolates it from the bottom contact. A reference cell for the planar InAs *p*-*i*-*n* photodiode was also simulated to test our model. We included a contact layer (*n*-type, 3×10^{17} cm^{-3}) atop of InAs(Sb) nanowire segment (*n*-type, 1×10^{17} cm^{-3}) to induce a local electric field for higher internal quantum efficiency (IQE). More details about the unit cell schematics are presented in the Supplementary Information (SI.1). It is noteworthy to mention that the plasmonic gratings can be easily fabricated by angled metal deposition, as discussed in many earlier studies [5,6].

A diagram of the simulation process, composed of three major steps, is shown in figure 2. First, the electric field profile and optical absorption were solved in Lumerical FDTD. A 2.0 – 3.5 µm wavelength spectrum was selected for analysis, and the values for the refractive index n and the extinction coefficient k of InAs(Sb) were obtained from a previously reported study for input into the optical simulator [19]. Periodic boundary conditions were set on the x and y directions (simulating the nanowire array), while perfectly matched layer (PML) boundary conditions were applied above and below the nanowire array (z-direction) to simulate the infinitely extending air medium (above) and the substrate. The nanowire diameter was set as 200 nm, while the nanowire pitch P_x and P_y were both set to 1300 nm, a value which was obtained by optimization in a previous simulation study [20]. The thickness of the Al_2O_3 passivation layer was 60 nm. To simulate the absorption of unpolarized light, we took note of the asymmetry of the nanowire photodetector in the x and y directions and set the incident light source to 45°-polarization, which contained both x-polarized and y-polarized components. Note that the electric field profiles solved by the optical simulator for each wavelength were based on a unique and consistent optical input power (in arbitrary units). Then, the simulated electric field and optical generation profiles from 2.0 – 3.5 µm in finite-difference time-domain (FDTD) mesh grids were interpolated into the finite-element mesh (FEM) grids so that it could be imported into the electrical simulator (Synopsys Sentaurus TCAD). Since the electrical simulator does not allow computation of current at 0 V applied bias, we used 0.0001 V to represent photovoltaic operation mode. Then, the imported electric field profiles are converted to optical generation profiles and the electrical simulator solves the drift-diffusion and continuity equations to output the dark and light current. A schematic diagram of the modeling process is given in SI.2.

2.2. Parameter settings

All the simulations were performed at 300 K. To study the theoretical, or ideal, spectral response (R and D^*) of the nanowire photodetectors, we used the electrical material properties of thin-film InAs for nanowires [21]. Note that the bandgap of InAs nanowires grown by catalyst-free selective-area mode is between 0.477 – 0.496 eV, much different from the zinc-blende InAs bandgap of 0.364 eV at 300 K [22]. This is mainly due to a high density of rotational twins, i.e., crystal phase switches between zinc-blende and wurtzite, which is commonly observed in InAs nanowires grown by selective-area growth mode [22,23]. Therefore, we intentionally added antimony into InAs during growth to form $InAs_{0.95}Sb_{0.05}$ and achieve the same bandgap as that of thin-film InAs [8,23,24]. When exploring the impact of nanowire material quality on spectral response, we varied carrier (electron and hole) mobility (μ_e and μ_h) and Shockley-Read-Hall (SRH) bulk carrier lifetime (τ_{SRH}). We have previously shown in several studies that the carrier dynamics in 3-D nanowires are highly dependent on material properties [25,26]. To make the photoresponse modeling more valid, we accounted for nonradiative recombination at surfaces when simulating nanowire photodetectors. Note that we used Al_2O_3 layers instead of standard *in-situ* large bandgap III-V materials as passivation shells. It has been recently demonstrated that by using *ex-situ* Al_2O_3 passivation the surface recombination velocity (v_S) of InAsSb nanowires can be significantly suppressed by two orders from a level of 10^5 cm/s to a level of 10^3 cm/s or less [14]. The passivation shells were conformally formed by atomic-layer deposition (ALD) at 200°C. Here, we kept v_S of InAsSb/Al_2O_3 interface fixed at 1×10^3 cm/s. Table S1 in SI.3 shows a list of material parameters applied in the model related to doping levels, mobilities, nonradiative recombination, and more. Some parameters such as carrier mobility and carrier lifetime were obtained by fitting the dark current of the InAs *p-i-n* diode with a mesa size of 400 µm [3], and those values were reasonably comparable to the results from other references [21,27]. All other material parameters were taken from the material database of the TCAD simulator.

2.3. Spectral response of nanowire photodetectors

The responsivity is given by

$$\sigma(\lambda) = \frac{I_{ph}(\lambda)}{P(\lambda)} = \frac{I_{ph}(\lambda)}{\int G(x,y,z,\lambda)dV/A(\lambda)} \quad (2)$$

where I_{ph} is the output photocurrent ($I_{ph} = I_{total} - I_{dark}$), P is the input power, G is the optical generation rate for a specific incident light wavelength in units of cm^{-3} s^{-1}, and A is wavelength dependent optical absorptance. To obtain the total input power at a certain wavelength, we integrated G over the InAsSb nanowire segment and then divided the integral sum by $A(\lambda)$. In this case, we only needed to calculate the input power once, because the power was kept fixed in the optical simulations by FDTD for the entire wavelength regime. Finally, we normalized I_{dark} by the nanowire junction area to get J_{dark} and then calculated D^* by eq. 1. Here, we assume that the detectors work in the quantum regime (not limited by Johnson or thermal noise).

2.4. Model validation

To demonstrate the validity of the 3-D photoresponse model, we also simulated the spectral response of a reference planar InAs *p-i-n* photodiode in photovoltaic mode [3]. As detailed in SI.3, the InAs *p-i-n* photodiode was composed of a n^+-InAs top contact layer (1×10^{18} cm^{-3}, 2 µm), a *i*-InAs layer (7×10^{14} cm^{-3}, 2 µm), and a p^+-InAs bottom contact layer (1×10^{18} cm^{-3}, 2 µm). The reported responsivity at 2 µm was about 0.75 A/W for (mesa size of 400 µm), where the effect of surface recombination on mesa sidewalls was minimal (hence the surface was assumed ideal in the simulation). Similarly, with the simulation process that we used above, the calculated photocurrent (at an input power of 2×10^{-10} W) was 1.69×10^{-10} A at 2 µm, yielding a responsivity of 0.85 A/W, very close to the experimentally measured value of 0.75 A/W (the value was calibrated by a 2 µm laser). More simulation results are presented in SI.4.

3. Results and discussion

We first investigate the ideal spectral response of the InAsSb-InP nanowire-plasmonic heterojunction photodiode, as shown in figure 3. We also show the simulation result of an InAsSb-InAs nanowire heterojunction photodiode, i.e., on InAs substrate, as reference. Here, the exposed nanowire height is kept fixed at 800 nm. Figure 3a illustrates the *x*-polarized and *y*-polarized electric profiles at 3 µm. Since the surface plasmon mode is tightly confined at the nanowire tip, the photocarriers (electrons) can be quickly

swept to the 3-D contacts. Furthermore, these photocarriers are entirely isolated from the interface with ambient air due to the Al_2O_3 passivation layer, and thus the impact of surface recombination on photocurrent, or responsivity, is much lower. Note that the Al_2O_3 passivation layers fully cover the nanowire sidewalls, and only the top facets are exposed to form the contacts. This is advantageous because: (1) the high bandgap oxide passivation layers can completely prevent depletion of top nanowire segments by the metal contacts under applied bias; (2) the *ex-situ* Al_2O_3 deposition by ALD is more robust and controllable than the *in-situ* passivation technique; thus the thickness of Al_2O_3 layer can be accurately controlled by deposition time, making it much easier to grow a thicker shell without formation of dislocations at the nanowire-oxide interfaces; and (3) the "effective" thickness of nanowire can be enhanced by forming a thick Al_2O_3 shell, resulting in greater modal field confinement in the nanowire core and hence less overlap in the metallic grating, which leads to higher optical absorption. Although it is common to embed nanowire arrays in the BCB layer and use indium tin oxide (ITO) as the top contact layer (instead of plasmonic light couplers), ITO is not transparent over 2.5 µm wavelength and the contact resistance is high. Therefore, it is still advantageous to use plasmonic gratings, despite the absorption loss in the gold layers.

Figure 3b displays a comparison of optical absorption between the InAsSb-InP nanowire photodiode array and the planar InAs photodiode. Clearly, the planar device offers a much higher optical absorption (~70%) across the entire spectrum (except the regime close to the bandgap cutoff) due to their thicker absorbers (thickness ~14 µm). In contrast, the absorption of nanowires mostly relies on the excited surface plasmon wave on the exposed nanowire top segments (~1 µm). At the plasmonic peaks, the nanowire detector absorption can reach up to ~15% (at 3 µm wavelength), roughly 4 – 5 times less than that of thin-film devices. By assuming the same IQE for both types of photodiodes, we estimate that the responsivities of nanowire devices will be lower. The absorption peak at 3 µm results from the fundamental surface plasmon mode (SP_{01}) resonance.

We move on to compute the spectral response by incorporating the 3-D optical profile into the 3-D electrical model (figure 2), Again, to solve the photocurrent in photovoltaic mode, we apply 0.0001 V to the detectors, which to some extent represents a random fluctuation of "zero" voltage in measurement

setups. Figure 3c presents the simulated responsivity spectra of the nanowire photodiodes (on both InP and InAs substrates) and planar InAs *p-i-n* photodiode. The calculated external quantum efficiency (EQE) is shown in SI.5. The responsivities of nanowire photodiodes on InP and InAs substrate are the same, confirming that the substrate optical property has very little impact of surface plasmonic resonance and hence resultant photocurrent is mostly determined by the properties of nanowire segments. It is immediately apparent that the responsivity of the nanowire photodiodes is lower than that of the planar device. The reasons are obvious: (1) the optical absorption of nanowire photodetectors is more than 4 – 5 times lower, as discussed earlier, and (2) the IQE of the nanowire devices is lower. A lower IQE of nanowire photodiodes results from a much thinner depletion region due to their high unintentional doping (*n*-type). As for typical planar InAs *p-i-n* photodiodes the doping of the intrinsic layer can be precisely controlled to low levels ($\sim 10^{14} - 10^{15}$ cm^{-3}). While for bottom-up nanowire photodetectors, it is impractical to achieve such low doping level, which is mostly limited by the epitaxial capability. Thus, it is reasonable for InAsSb-InP nanowire photodiodes to have a lower responsivity and IQE than planar photodiodes.

We also calculate the nanowire photodiode D^* at 0.0001V (photovoltaic mode, figure 3d). A comparison of dark current used to calculate D^* is listed in Table 1. Remarkably, the room-temperature D^* of InAsSb-InP nanowire heterojunction photodiode can achieve over 3.5×10^{10} cm $Hz^{1/2}$ W^{-1} at plasmonic mode (SP_{01}) resonance peak wavelength of 3.0 µm. This D^* value outperforms that of commercial uncooled InAs *p-i-n* photodiodes and approaches that of the cryogenically cooled (77 K) InSb *p-i-n* photodiodes. Furthermore, we observe that the D^* of InAsSb-InAs nanowire photodiode is lower than that of InAsSb-InP nanowire photodiode. This is due to InAsSb-InAs nanowire photodiode having one-order higher dark current than that of the InAsSb-InP nanowire photodiode, which results from the higher minority carrier diffusion current stemming from the lower bandgap InAs substrate compared to that of InP substrate. Nevertheless, the D^* of InAsSb-InAs nanowire photodiode is higher than that of planar InAs photodiode at wavelengths spanning 2.5 – 3.1 µm. Such results clearly demonstrate the potential of InAsSb-based nanowire photodetectors in breaking the trade-off between high responsivity and low dark current as the reduction in dark current is much greater than that of responsivity. Further device structure optimization of

InAsSb-based nanowire photodetector can lead to a higher D^* that spans the entire MWIR spectrum between 3 – 5 μm.

Furthermore, as shown in figure 4, the detection peaks can be tuned simply by varying the exposed nanowire height. Note that this design is compatible with the practical fabrication process of nanowire devices, since the height of the individual nanowire array can be lithographically controlled during the BCB etch-back process. Clearly, the D^* peaks of surface plasmon resonance (SP_{01}) red-shift with increasing nanowire exposed height from 600 nm to 1200 nm. Also, all plasmonic peaks show over one-order higher D^* than the peak D^* of the uncooled planar InAs *p-i-n* photodiodes. Thus, it is possible to efficiently design a focal plane array comprised of InAs(Sb) nanowire arrays with different exposed heights to achieve high detectivity spanning 2.0 – 3. 5 μm. This further opens the possibility of developing nanowire-plasmonic multichannel detectors for multispectral and hyperspectral imaging applications. Also note that the cutoff wavelength can be extended beyond 3.5 μm by using InAsSb nanowires with higher antimony compositions.

Finally, we take the nanowire material quality into account and analyze the impact of carrier mobility and carrier lifetime on peak D^*. It is known that the quality of nanowire materials might not be as good as bulk materials. For instance, due to the rotational twins and local defects formed during epitaxy, the carrier mobility (μ_e) and SRH nonradiative recombination lifetime (τ_{SRH}) are degraded, respectively. Here, we keep the nanowire exposed height fixed at 800 nm and compute D^* with different combinations of mobility and lifetime: μ_e – 11000 cm^2 V^{-1}s^{-1} and 5000 cm^2 V^{-1}s^{-1}; τ_{SRH} – 1 μs, 0.1 μs, 0.01 μs, and 0.001 μs. Figure 5a shows the impact of τ_{SRH} on D^* with μ_e fixed at 11000 cm^2 V^{-1}s^{-1}. The difference between the D^* spectra is almost negligible when τ_{SRH} is greater than 0.01 μs. The relation between the peak D^* (at 3 μm) with μ_e and τ_{SRH} is further shown in figure 5b. We observe that when τ_{SRH} is greater than 0.01 μs, μ_e has negligible effect on peak D^*. In contrast, the peak D^* becomes more sensitive to the change of material properties when τ_{SRH} becomes smaller, within the scale of a few nanoseconds and lower. This is because most of the photogenerated carriers are tightly confined within nanoscale distance away from the 3-D contacts. Thus, the mean path to the contacts is much shorter than the carrier diffusion length defined by μ_e

and τ_{SRH}, and hence carriers diffuse to the contacts before being recombined in nanowire bulk or at the surface. Thus, the D^* becomes less sensitive to larger τ_{SRH} (greater than 0.01 μs) and variation in μ_e.

4. Conclusion

We demonstrated the feasibility of achieving high room-temperature D^* at SWIR and MWIR by using InAs(Sb)-InP nanowire-plasmonic heterojunction photodiodes. This device platform significantly suppressed the leakage current from G-R process and minority carrier diffusion. Meanwhile, the loss of optical absorber volume was compensated by using efficient 3-D plasmonic gratings for light coupling, thus breaking the trade-off between high responsivity and low dark current. We proved this concept by developing a 3-D computational model to numerically investigate the responsivity and D^* of InAs(Sb)-InP nanowire heterojunction photodiodes and compared the device performance with planar uncooled InAs *p-i-n* photodiodes and cryogenically cooled InSb *p-i-n* photodiodes. The resultant simulations showed that the plasmonic mode (SP_{01}) resonance peak D^* of 3.5×10^{10} cm $Hz^{1/2}W^{-1}$ at wavelength of 3.0 μm was about one-order higher than that of planar InAs photodiodes. Furthermore, we tuned the plasmonic peak D^* by simply varying the exposed height of the nanowire top segments, thus demonstrating multispectral capability. Finally, we investigated the impact of nanowire material quality on D^*. Our work shows that, through sophisticated optical and electrical design, nanowire-based photodetectors can demonstrate better performance than their planar device counterparts for photodetection at SWIR and MWIR.

Acknowledgements

We gratefully acknowledge the support for this research from the National Science Foundation (grant no. ECCS-1509801) and Sêr Cymru National Research Network in Advanced Engineering and Materials.

ORCID iDs

Dingkun Ren https://orcid.org/0000-0001-9470-1956

Supplementary Information

Schematics of unit cell, modeling process, material parameters used in the electrical simulations, validation of 3-D photoresponse model, simulated dark current, calculated external quantum efficiency.

Notes

The authors declare no competing financial interest.

References

[1] InGaAs photodiodes *Available from*:

https://www.hamamatsu.com/resources/pdf/ssd/ingaas_kird0005e.pdf

[2] InAs photovoltaic detectors *Available from*:

https://www.hamamatsu.com/resources/pdf/ssd/p10090-01_etc_kird1099e.pdf

[3] Zhou X, Meng X, Krysa A B, Willmott J R, Ng J S and Tan C H 2015 InAs photodiodes for 3.43 µm radiation thermometry *IEEE Sens. J.* **15** 5555-60

[4] Soibel A, Hill C J, Keo S A, Hoglund L, Rosenberg R, Kowalczyk R, Khoshakhlagh A, Fisher A, Ting D Z Y and Gunapala S D 2014 Room temperature performance of mid-wavelength infrared InAsSb nBn detectors *Appl. Phys. Lett.* **105** 023512

[5] Senanayake P, Hung C-H, Shapiro J, Lin A, Liang B, Williams B S and Huffaker D L 2011 Surface plasmon-enhanced nanopillar photodetectors *Nano Lett.* **11** 5279-83

[6] Lee W-J, Senanayake P, Farrell A C, Lin A, Hung C-H and Huffaker D L 2016 High quantum efficiency Nanopillar photodiodes overcoming the diffraction limit of light *Nano Lett.* **16** 199-204

[7] Ren D, Farrell A C, Williams B S Huffaker D L 2017 Seeding layer assisted selective-area growth of As-rich InAsP nanowires on InP substrates *Nanoscale* **9** 8220-8.

[8] Ren D, Farrell A C and Huffaker D L 2017 Selective-area InAsSb nanowires on InP for 3 – 5 µm mid-wavelength infrared optoelectronics *MRS Advances* **2** 3565-70

[9] Wei W, Bao X-Y, Soci C, Ding Y, Wang Z-L and Wang D 2009 Direct heteroepitaxy of vertical InAs nanowires on Si substrates for broad band photovoltaics and photodetection *Nano Lett.* **9** 2926-34

[10] Shin H W, Lee S J, Kim D G, Bae M-H, Heo J, Choi K J, Choi, W J, Choe, J-w and Shin, J C 2015 Short-wavelength infrared photodetector on Si employing strain-induced growth of very tall InAs nanowire arrays *Sci. Rep.* **5** 10764

[11] Thompson M D, Alhodaib A, Craig A P, Robson A, Aziz A, Krier A, Svensson, J, Wernersson, L-E, Sanchez and A M, Marshall, A R J 2016 Low leakage-current InAsSb nanowire photodetectors on silicon *Nano Lett.* **16** 182-7

[12] Svensson J, Anttu N, Vainorius N, Borg B M, Wernersson L-E 2013 Diameter-Dependent Photocurrent in InAsSb Nanowire Infrared Photodetectors *Nano Lett.* **13** 1380-5

[13] Ren D, Meng X, Rong Z, Cao M, Farrell A C, Somasundaram S, Azizur-Rahman K M, Williams B S and Huffaker D L 2018 Uncooled photodetector at short-wavelength infrared using InAs nanowire photoabsorbers on InP with p-n heterojunctions *Nano Lett.* to be submitted

[14] Ren D, Azizur-Rahman K M, Rong Z, Juang B-C, Somasundaram S, Farrell A C, Williams B S and Huffaker D L 2018 Developing uncooled InAsSb nanowire photodetector arrays with Al_2O_3 passivation for photodetection at mid-wavelegnth infrared *Nano Lett.* in preparation

[15] Azizur-Rahman K M and LaPierre R R 2015 Wavelength-selective absorptance in GaAs, InP and InAs nanowire arrays *Nanotechnology* **26** 295202

[16] Azizur-Rahman K M and LaPierre R R 2016 Optical design of a mid-wavelength infrared InSb nanowire photodetector *Nanotechnology* **27** 315202

[17] Robson M, Azizur-Rahman K M, Parent D, Wojdylo P, Thompson D A and LaPierre R R 2017 Multispectral absorptance from large-diameter InAsSb nanowire arrays in a single epitaxial growth on silicon *Nano Futures* **1** 035001

[18] Svensson J, Chen Y, Anttu N, Pistol M-E and Wernersson L-E 2017 Increased absorption in InAsSb nanowire clusters through coupled optical modes *Appl. Phys. Lett.* **110** 081104

[19] Adachi S 1989 Optical dispersion relations for GaP, GaAs, GaSb, InP, InSb, AlxGa1-xAs, and In1-xGaxAsyP1-y *J. Appl. Phys.* **66** 603040

[20] Physical properties of indium arsenide (InAs) *Available from*: http://www.ioffe.ru/SVA/NSM/Semicond/InAs

[21] Ren D, Rong Z, Cao M, Farrell A C, Meng X and Huffaker D L 2018 Feasibility of room-temperature mid-wavelength infrared photodetectors using InAsSb nanostructured photoabsorbers *Proc. SPIE* **10531** 105310Y

[22] Lin A, Shapiro J N, Scofield A C, Liang B L and Huffaker D L 2013 Enhanced InAs nanopillar electrical transport by in-situ passivation *Appl. Phys. Lett.* **102** 053115

[23] Ren D, Farrell A C and Huffaker D L 2018 Axial InAs(Sb) inserts in selective-area InAsP nanowires on InP for optoelectronics beyond 2.5 µm *Opt. Mater. Express* **8** 1075-81

[24] Farrell A C, Lee W-J, Senanayake P, Haddad M A, Prikhodko S V and Huffaker D L 2015 High-quality InAsSb nanowires grown by catalyst-free selective-area metal–organic chemical vapor deposition *Nano Lett.* **15** 6614-9

[25] Ren D, Scofield A C, Farrell A C, Rong Z, Haddad M A, Laghumavarapu R B, Liang B and Huffaker D L 2018 Exploring time-resolved photoluminescence for nanowires using a three-dimensional computational transient model *Nanoscale* **10** 7792-802

[26] Ren D, Rong Z, Somasundaram S, Azizur-Rahman K M, Liang B and Huffaker D L 2018 A three-dimensional insight into correlation between carrier lifetime and surface recombination velocity for nanowires *Nanotechnology* submitted

[27] Sun W, Lu Z, Zheng X, Campbell J C, Maddox S J, Nair H P and Bank S R 2013 High-gain InAs avalanche photodiodes *IEEE J. Quatum Electron.* **49** 154-61.

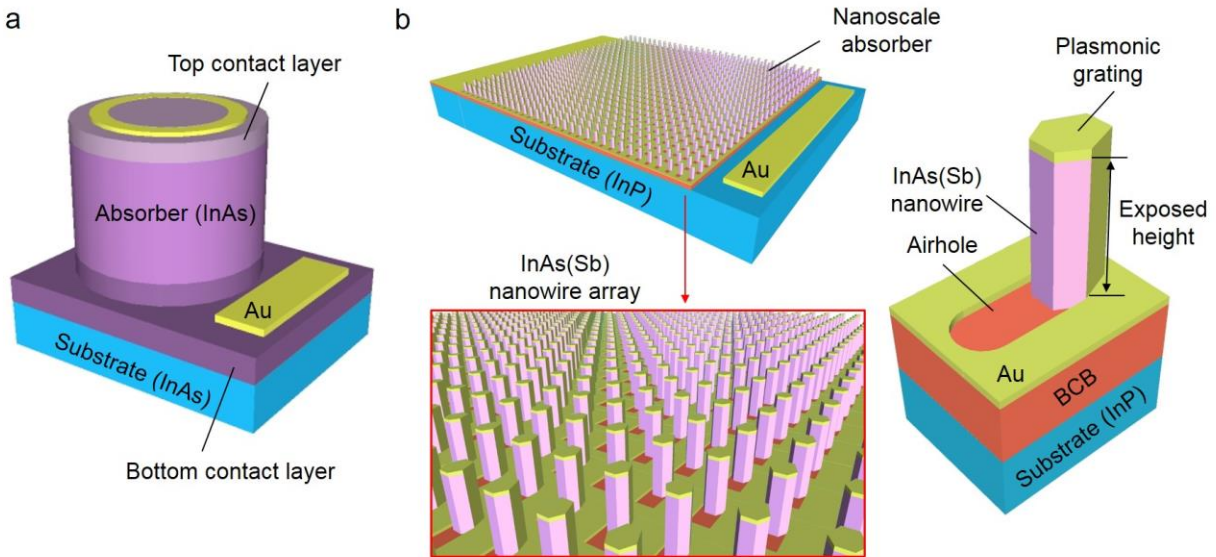

Figure 1. Schematic diagrams of (a) a planar InAs *p*-*i*-*n* photodiode with a cylindrical mesa as photoabsorber and (b) a nanowire-based InAs(Sb)-InP heterojunction photodiode with a InAs(Sb) nanowire array as photoabsorber. The nanowire segments and the substrate form *p*-*n* heterojunctions. Here, InAs(Sb) nanowires are *n*-type and InP substrate is *p*-type. The exposed height of the nanowire top segment is labelled.

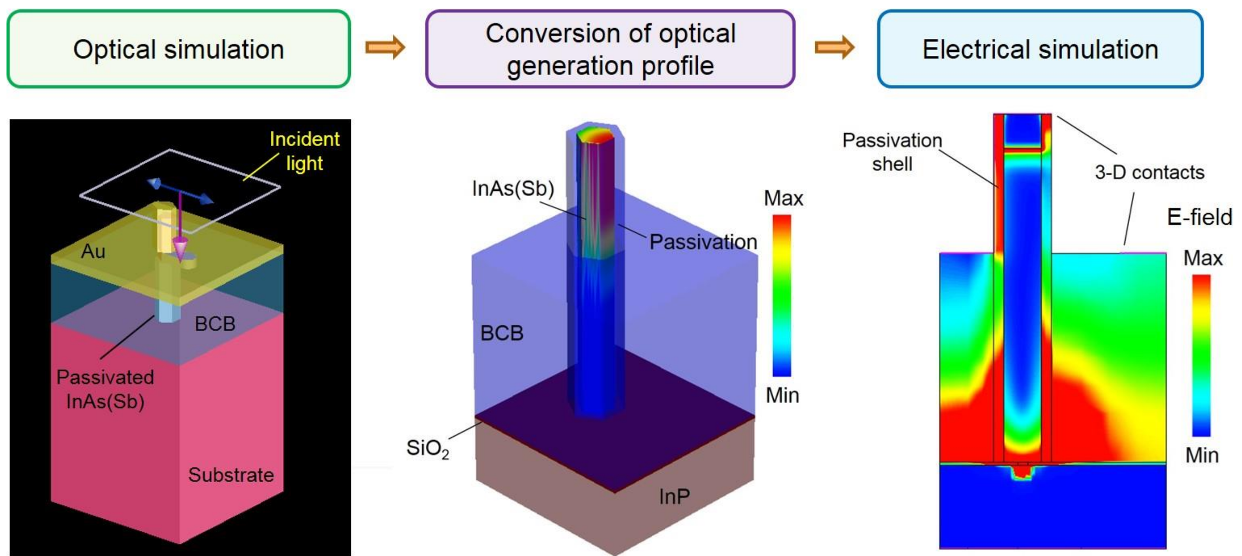

Figure 2. Schematic diagram of simulation process, which is composed of three major steps: (1) optical simulation by FDTD, (2) conversion of optical profile from FDTD mesh to FEM mesh, and (3) electrical simulation by FEM.

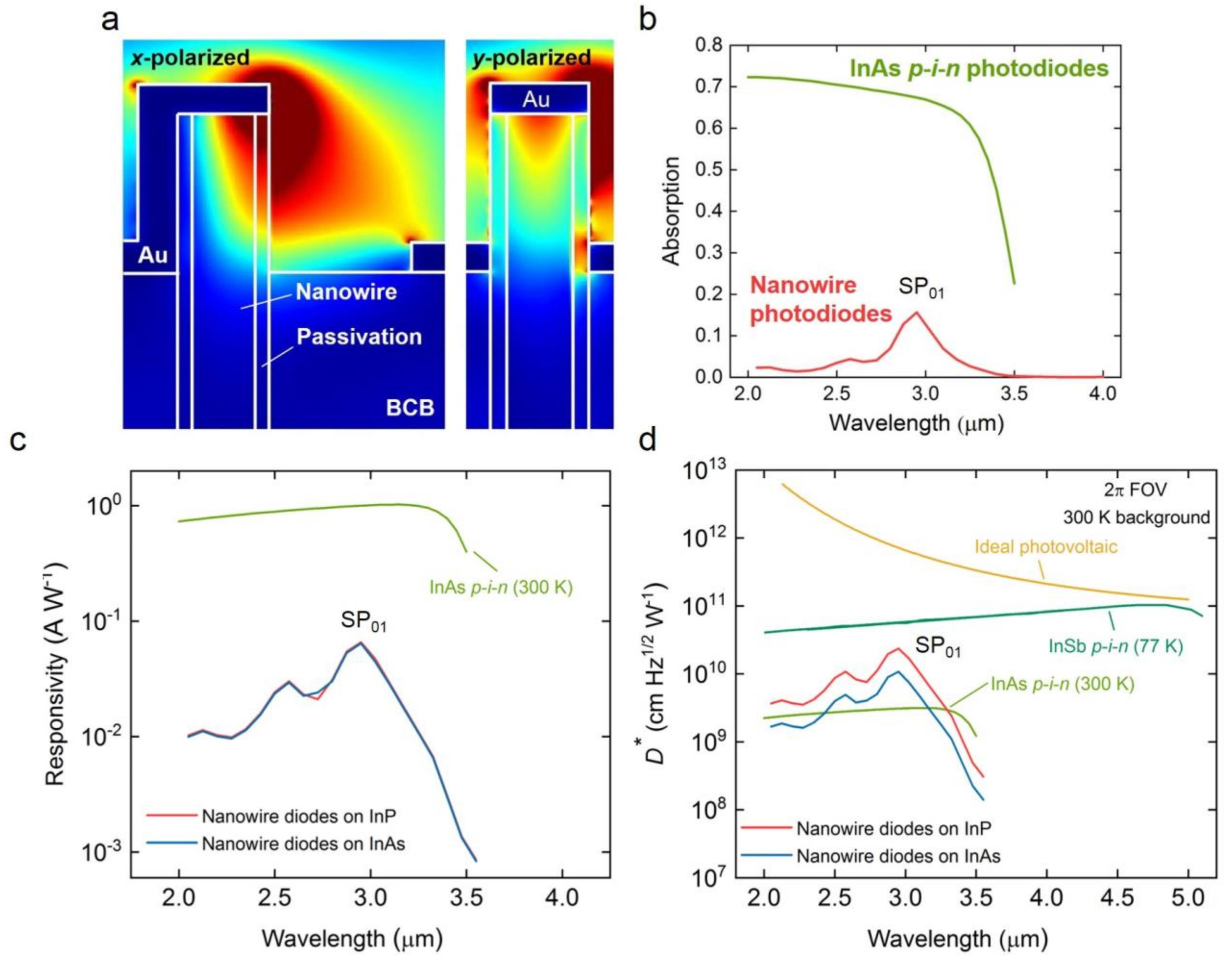

Figure 3. Simulated spectral response of InAs(Sb) nanowire photodiodes. (a) Optical generation: x-polarized and y-polarized electric profiles at 3 μm. (b) Optical absorption of InAsSb nanowire photodiodes and planar InAs photodiodes. (c) Responsivity of nanowire photodiodes on InP and InAs substrates. (d) D^* of nanowire photodiodes on InP and InAs substrates, where D^* from reference cells of commercial uncooled InAs photodiodes and cryogenically cooled (77 K) InSb photodiodes are also presented.

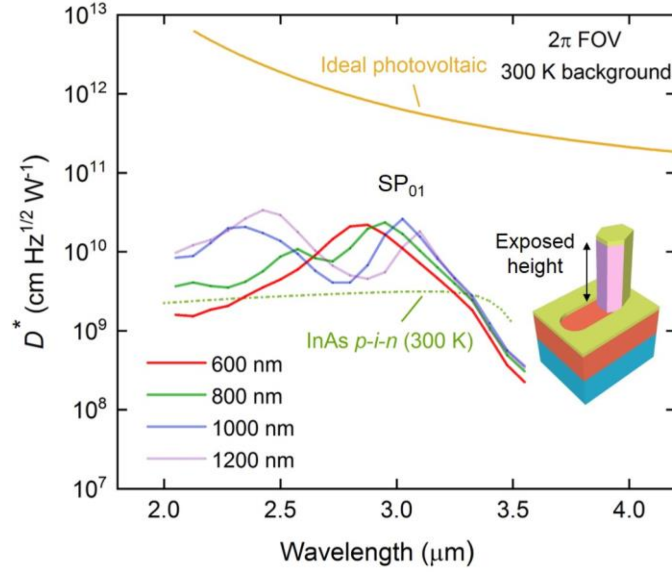

Figure 4. D^* as a function of the exposed nanowire height from 600 nm to 1200 nm for nanowire core diameter and array pitch of 200 nm and 1300 nm respectively. The diameter and array pitch were optimized in a previous simulation study. A 60 nm thick Al_2O_3 passivation layer was further used to passivate the nanowire.

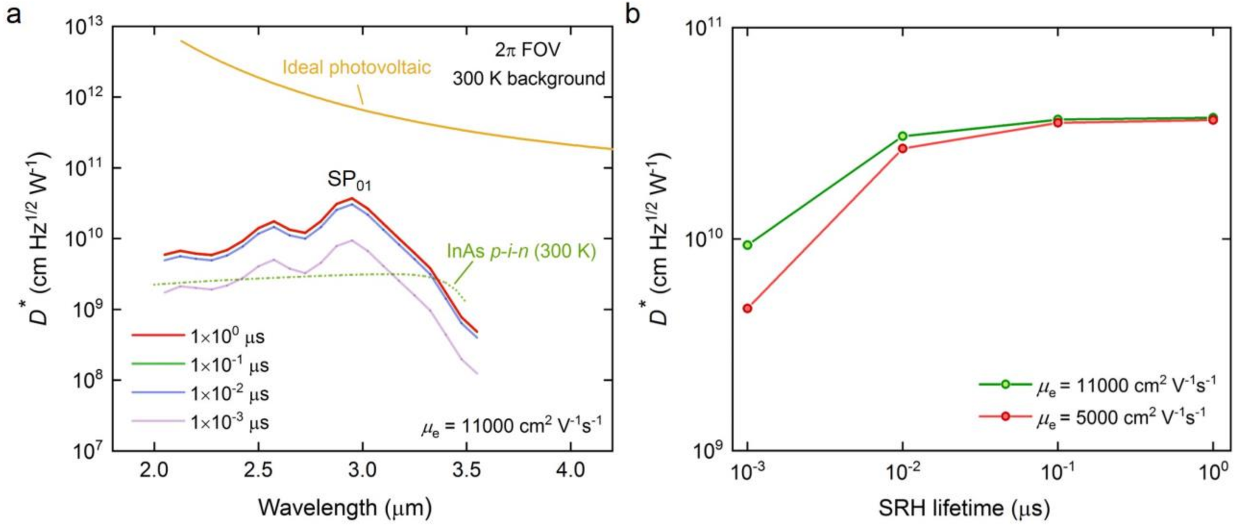

Figure 5. Impact of nanowire material quality on D^*. (a) Spectra of D^* as a function of τ_{SRH} (1 μs, 0.1 μs, 0.01 μs, and 0.001 μs). μ_e is kept fixed at 11000 cm^2 V^{-1}s^{-1}. (b) Peak D^* (at 3 μm) as a function of μ_e (11000 cm^2 V^{-1}s^{-1} and 5000 cm^2 V^{-1}s^{-1}) and τ_{SRH} (1 μs, 0.1 μs, 0.01 μs, and 0.001 μs).

Table 1. Comparison of the simulated dark current density J_{dark} at 0.0001 V (photovoltaic mode).

Devices	Absorber thickness (μm)	J_{dark} (A cm^{-2})
InAs(Sb)-InP nanowire heterojunction photodiodes	2	~2.7×10^{-6}
InAs(Sb)-InAs nanowire heterojunction photodiodes	2	~1.1×10^{-4}
InAs *p*-*i*-*n* homojunction photodiodes (references)	4 – 8 [2,3,27]	~2.0×10^{-1}